Mechanisms of enhanced drug delivery in brain metastases with focused ultrasound-induced blood–tumor barrier disruption

Costas D. Arvanitis[a,b,1,2], Vasileios Askoxylakis[c,1], Yutong Guo[a], Meenal Datta[c,d], Jonas Kloepper[c,3], Gino B. Ferraro[c], Miguel O. Bernabeu[e], Dai Fukumura[c], Nathan McDannold[f], and Rakesh K. Jain[c,2]

[a]School of Mechanical Engineering, Georgia Institute of Technology, Atlanta, GA 30332; [b]Department of Biomedical Engineering, Georgia Institute of Technology, Atlanta, GA 30332; [c]Edwin L. Steele Laboratories, Department of Radiation Oncology, Massachusetts General Hospital, Harvard Medical School, Boston, MA 02114; [d]Department of Chemical and Biological Engineering, Tufts University, Medford, MA 02155; [e]Centre for Medical Informatics, Usher Institute, University of Edinburgh, Edinburgh EH16 4UX, United Kingdom; and [f]Department of Radiology, Brigham and Women's Hospital, Harvard Medical School, Boston, MA 02115

Contributed by Rakesh K. Jain, July 28, 2018 (sent for review April 27, 2018; reviewed by Katherine W. Ferrara and Richard J. Price)

Blood–brain/blood–tumor barriers (BBB and BTB) and interstitial transport may constitute major obstacles to the transport of therapeutics in brain tumors. In this study, we examined the impact of focused ultrasound (FUS) in combination with microbubbles on the transport of two relevant chemotherapy-based anticancer agents in breast cancer brain metastases at cellular resolution: doxorubicin, a nontargeted chemotherapeutic, and ado-trastuzumab emtansine (T-DM1), an antibody–drug conjugate. Using an orthotopic xenograft model of HER2-positive breast cancer brain metastasis and quantitative microscopy, we demonstrate significant increases in the extravasation of both agents (sevenfold and twofold for doxorubicin and T-DM1, respectively), and we provide evidence of increased drug penetration (>100 vs. <20 μm and 42 ± 7 vs. 12 ± 4 μm for doxorubicin and T-DM1, respectively) after the application of FUS compared with control (non-FUS). Integration of experimental data with physiologically based pharmacokinetic (PBPK) modeling of drug transport reveals that FUS in combination with microbubbles alleviates vascular barriers and enhances interstitial convective transport via an increase in hydraulic conductivity. Experimental data demonstrate that FUS in combination with microbubbles enhances significantly the endothelial cell uptake of the small chemotherapeutic agent. Quantification with PBPK modeling reveals an increase in transmembrane transport by more than two orders of magnitude. PBPK modeling indicates a selective increase in transvascular transport of doxorubicin through small vessel wall pores with a narrow range of sizes (diameter, 10–50 nm). Our work provides a quantitative framework for the optimization of FUS–drug combinations to maximize intratumoral drug delivery and facilitate the development of strategies to treat brain metastases.

focused ultrasound | brain tumor | pharmacokinetics | blood–brain/blood–tumor barrier | drug transport

Brain metastases (BMs) have poor prognosis. The incidence of cerebral metastases varies with tumor type and is on the rise, especially as modern therapies improve extracranial disease control. Breast cancer, lung cancer, and melanoma are among the tumor types associated with high brain-metastatic prevalence (1, 2). Overall, it is estimated that 10–20% of cancer patients develop BM (2). Clinical treatment is in most cases palliative (2), whereas the prognosis is affected by various factors, including the number of BMs, the tumor type, the presence of active extracranial disease, and the patient's age and performance status (3). Survival rates are in most cases on the order of months (1, 2).

The blood–brain barrier (BBB) is often considered a challenge in the treatment of brain malignancies, since it may affect drug delivery and penetration (4–7). However, abnormal angiogenesis in tumors, due to an overproduction of proangiogenic factors (8), leads to the formation of blood vessels that lack normal physiological structure, resulting in a compromised BBB, which is referred as the blood–tumor barrier (BTB). In contrast to the normal BBB, the leaky BTB often allows for the extravasation of larger molecules, including antibodies (4, 9, 10). However, the BTB permeability is characterized by heterogeneity and varies not only between BMs but also within a lesion (5). As a result, it remains largely unclear whether the amount of drug that is able to penetrate into BM is sufficient to control tumor growth; furthermore, some malignant foci may grow around vessels with intact BBB—via vessel "co-option"—thus limiting drug delivery (8, 11). As a result, increased efforts in recent years have focused on approaches to transiently disrupt the BBB/BTB to enhance delivery of therapeutics into primary and metastatic brain tumors

Significance

Improved penetration along with accurate prediction and mechanistic understanding of anticancer agent delivery across the blood–brain/blood–tumor barrier (BBB/BTB) are essential for the rational development of effective therapeutic strategies in intracranial malignancies. In this study, we provide insights in drug pharmacokinetics in brain metastases after focused ultrasound-induced BBB/BTB disruption by integrating quantitative microscopy with mathematical modeling. We demonstrate that focused ultrasound-induced BBB/BTB disruption contributes to enhanced interstitial convective transport in solid tumors, in addition to alleviating vascular barriers, and provide evidence of improved penetration of nontargeted and antibody-targeted chemotherapies. Together, our work provides a unified framework for prospective, quantitative, and mechanistic investigation of the penetration of anticancer drugs across the BBB/BTB in brain tumors.

Author contributions: C.D.A., V.A., and R.K.J. designed research; C.D.A., V.A., Y.G., M.D., J.K., M.O.B., D.F., and R.K.J. performed research; C.D.A., V.A., G.B.F., N.M., and R.K.J. contributed new reagents/analytic tools; C.D.A., V.A., Y.G., M.D., and R.K.J. analyzed data; and C.D.A., V.A., Y.G., M.O.B., and R.K.J. wrote the paper.

Reviewers: K.W.F., Stanford University; and R.J.P., University of Virginia.

Conflict of interest statement: R.K.J. received an honorarium from Amgen and consultant fees from Merck, Ophthotech, Pfizer, SPARC, SynDevRx, and XTuit; owns equity in Enlight, Ophthotech, SynDevRx, and XTuit; served on the Board of Directors of XTuit; and serves on the Boards of Trustees of Tekla Healthcare Investors, Tekla Life Sciences Investors, Tekla Healthcare Opportunities Fund, and Tekla World Healthcare Fund. Neither any reagent nor any funding from these organizations was used in this study.

[1]C.D.A. and V.A. contributed equally to this work.

[2]To whom correspondence may be addressed. Email: costas.arvanitis@gatech.edu or jain@steele.mgh.harvard.edu.

[3]Present address: Department of Oncology, Centre Hospitalier Universitaire Vaudois, CH-1011 Lausanne, Switzerland.

This article contains supporting information online at www.pnas.org/lookup/suppl/doi:10.1073/pnas.1807105115/-/DCSupplemental.

Published online August 27, 2018.

(12). Different approaches have been developed, including chemical disruption of the BBB/BTB via administration of vasoactive compounds such as bradykinin or adenosine receptor agonists (13–15), systemic administration of polymeric nanoparticles and microparticles (16), or physical methods via implantation of a delivery system directly into the tumor bed (17). While these strategies may improve drug uptake in brain tumors, they have important limitations: Chemical disruption of BBB may induce generalized disruption of the BBB, whereas physical methods are invasive (12).

Focused ultrasound (FUS) in combination with i.v. administered microbubbles is a promising local, minimally invasive, and transient physical method for targeted BBB/BTB disruption (18–20). Extensive preclinical research has shown that FUS can lead to an average of 4-fold increase in the delivery of small chemotherapeutic agents, 3.5-fold increase in the delivery of monoclonal antibodies, and 5.5-fold increase in the delivery of nanoparticle drug formulations in brain tumors (*SI Appendix*, Table S1). This improvement in the delivery of anticancer agents has led to increase of median survival time in multiple orthotopic murine tumor models, supporting the therapeutic potential of this strategy (*SI Appendix*, Table S1).

While the promising preclinical data have led to phase I clinical trials (21), there is a limited understanding of how physicochemical drug properties, such as size, molecular weight, and cell binding affinity, influence the effects of FUS-mediated BBB/BTB disruption on interstitial transport and cellular uptake in the highly heterogeneous tumor microenvironment. This is mainly due to the fact that previous studies largely rely on (*i*) methods that require tissue homogenization (e.g., HPLC), which lacks spatial information; and (*ii*) use of imaging surrogates (e.g., MRI contrast agents, radiolabeled molecules for positron emission tomography) that have limitations in regard to resolution and distinction between intravascular and extravascular drug kinetics, and cellular uptake (*SI Appendix*, Table S1). Moreover, the previously reported weak correlation between intratumoral drug uptake and K_{trans} (*SI Appendix*, Table S1), a bulk transport parameter obtained using dynamic contrast-enhanced MRI, is dependent on both capillary permeability and perfusion. All of these limitations call for improved approaches to quantify the relative contribution of different transport mechanisms (e.g., role of convection versus diffusion, cellular uptake) to explain the reported increased extravasation after FUS-BBB/BTB disruption. Such methods could also provide additional insights regarding the potential of FUS to reduce the interstitial fluid pressure (IFP) (22) in brain tumors, as it has been shown to do in extracranial malignancies (23). A reduction in IFP could reestablish the pressure gradients required for effective interstitial convective transport (24). Finally, the impact of FUS-BBB/BTB disruption on transmembrane transport and cellular drug uptake is largely unexplored.

In addition to experimental methods, mathematical modeling is an important tool for elucidating mechanisms governing drug transport (22, 25). In particular, physiologically based pharmacokinetic (PBPK) modeling has provided important insights into (*i*) the impact of anticancer agents' physicochemical properties on intratumoral penetration and retention (25–28), (*ii*) the contribution of intratumoral heterogeneity (e.g., aberrant vascularity) to significant drug concentration heterogeneity found in solid tumors (29), and (*iii*) the importance of drug administration protocols (30, 31) and vascular remodeling strategies (32, 33) in improving drug accumulation. Mathematical models have also been employed to analyze interstitial drug transport using data extracted from quantitative imaging analysis (25, 32, 34, 35). Despite this progress, to date there is no comprehensive model based on experimental data that capture agent-specific transport parameters at the cellular level in brain tumors after FUS. It also remains largely unclear how the determinants of intratumoral drug distribution extracted by existing PBPK models are affected by FUS-BBB/BTB disruption. Moreover, little attention has been paid to characterizing the intrinsic variability underpinning drug PK via mathematical modeling (36). Taken together, these aspects may open new ways of improving therapeutic interventions, such as FUS-BBB/BTB disruption.

Here, we combine noninvasive, high-resolution imaging techniques that provide molecular, cellular, and structural insights with mathematical modeling to investigate agent-specific drug transport after FUS-mediated BBB/BTB disruption in the brain tumor microenvironment. Specifically, we determine the intratumoral penetration and cellular uptake of two different chemotherapy-based drugs: the nontargeted low–molecular-weight chemotherapeutic agent doxorubicin and the antibody–drug conjugate adotrastuzumab emtansine (T-DM1), which represents a targeted chemotherapy. We perform our studies in clinically relevant mouse models of BMs from HER2-positive breast cancer using intravital multiphoton microscopy and immunofluorescent staining, respectively. Moreover, we combine the experimental data with drug-specific PBPK model to estimate the relevant drug transport parameters, including BBB/BTB effective diffusive permeability, interstitium diffusion coefficient, hydraulic conductivity, vessel and interstitium porosity (fraction of surface area occupied by pores), cellular binding, and transmembrane kinetics and uptake (with separate formulation for the nontargeted and targeted agents), and determine their influence on interstitial drug transport after FUS-BBB/BTB disruption. Our findings show that FUS contributes to enhanced interstitial convective transport in solid tumors, in addition to alleviating vascular barriers. The proposed mathematical framework provides a platform for the development of therapeutic protocols, aiming to maximize drug penetration and uptake in BMs following FUS-mediated BBB/BTB disruption.

Results

FUS in Combination with Microbubbles Improves Doxorubicin Uptake and Penetration in HER2-Positive Breast Cancer BMs Through Promotion of Convective Interstitial Transport. *HER2*-amplified BT474 breast cancer cells were genetically engineered to express green fluorescence protein (GFP) for tumor cell imaging, and secreted gaussia luciferase (BT474-GFP-Gluc) for tumor burden evaluation as previously described (9, 10, 37). The focus of a custom-built FUS system, mounted on a 3D positioning system with submillimeter precision, was directed to the targeted region of orthotopically implanted BT474-GFP-Gluc tumors in the brain using needle guidance in mice bearing transparent cranial windows (Fig. 1*A*). Dissemination analysis of the 960-Da impermeable dye trypan blue by gross histology after successive sonications in four nonoverlapping target regions, separated by 2 mm, in healthy non–tumor-bearing mice indicated that 480-kPa peak negative pressure (based on absolute characterization of the FUS system; *SI Appendix*, *Methods*, section 1) was sufficient to attain consistent FUS-induced BBB/BTB disruption without inducing hemorrhage (Fig. 1*A*). Hence, this pressure was employed throughout the work presented here.

After we established the exposure conditions and targeting accuracy, we evaluated the PK of the nontargeted chemotherapeutic doxorubicin (580 Da). To assess doxorubicin temporal and spatial distribution immediately after FUS-mediated BBB/BTB disruption, we performed intravital imaging of BT474-GFP-Gluc brain tumors in the mouse cranial window model (Fig. 1 *B* and *C*). Multiphoton microscopy showed a remarkable increase in doxorubicin extravasation after FUS-BBB/BTB disruption compared with non-FUS over a short period of time (12 min) (Fig. 1*C*). Quantification of the multiphoton microscopy data revealed sevenfold higher doxorubicin concentration/fluorescence in the extravascular regions after FUS-BBB/BTB disruption compared with non-FUS (Fig. 2 *A* and *B*) ($P < 0.05$).

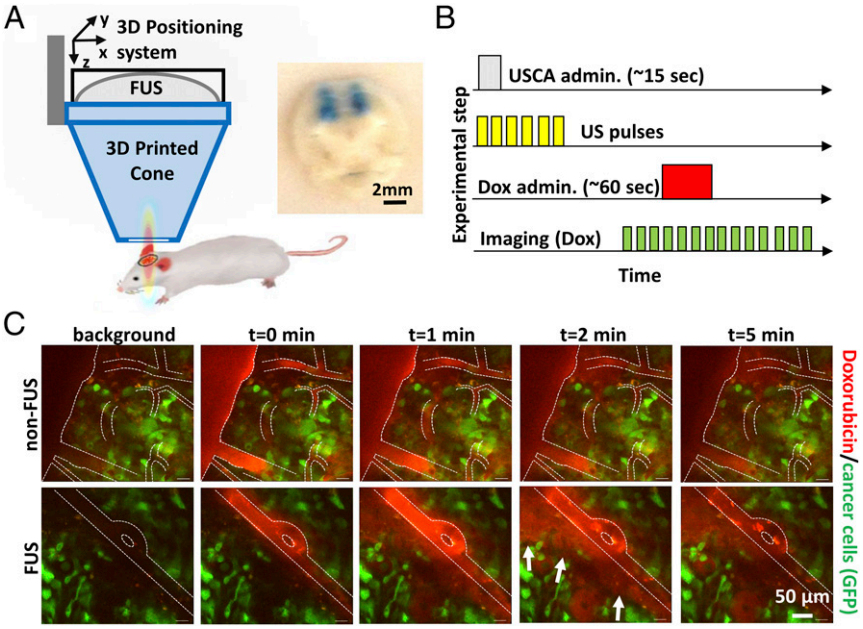

Fig. 1. FUS enhances doxorubicin extravasation in BT474-Gluc brain tumors. (*A*) FUS system and experimental setup. (*Inset*) Image of trypan blue extravasation in gross pathology of a coronal plane section after FUS-BTB disruption in healthy mice (480-kPa peak negative pressure). (*B*) Schematic illustration of the drug administration protocol. Ultrasound contrast agent (USCA–Definity; Lantheus Medical Imaging) was administered as a bolus. (*C*) Representative sequential images from intravital multiphoton microscopy of doxorubicin distribution in the breast cancer BM model with (*Lower*) and without (*Upper*) FUS-BTB disruption. Red, doxorubicin autofluorescence; green, GFP-positive BT474-Gluc cancer cells.

In addition, more than a fivefold increase in doxorubicin penetration distance was found after FUS compared with non-FUS (>100 vs. <20 µm, based on doxorubicin penetration regression) (Fig. 2*C*). Of note, assessment of the temporal evolution of the drug concentration (line profile) in the interstitial space after FUS revealed drug distribution at length and time scales that suggest significant contribution from enhanced convective transport (Fig. 2*D*) (~60 µm, 40 s; uniform drug profile displays

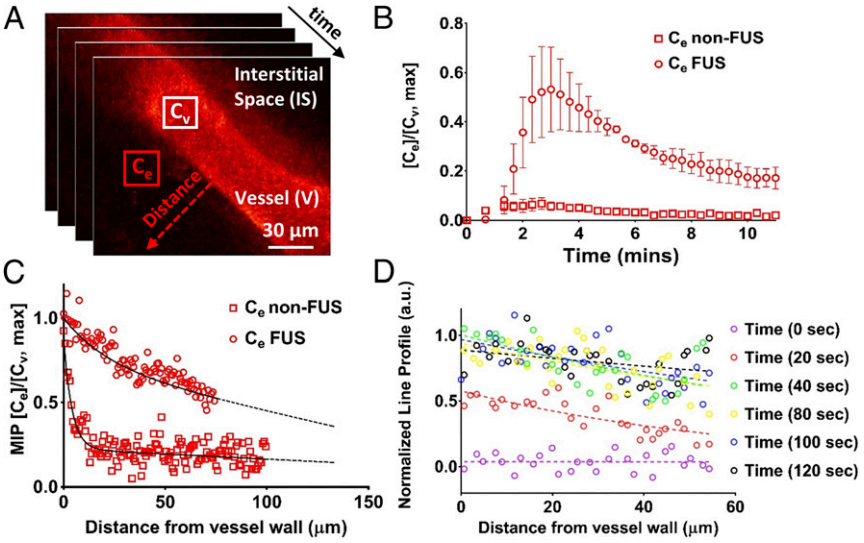

Fig. 2. FUS enhances doxorubicin (Dox) penetration and promotes convective transport in BT474-Gluc brain tumors. (*A*) Sequential intravital multiphoton microscopy of Dox autofluorescence. Approximately 50 images were acquired at 20-s intervals during i.v. injection of 150 µL of Dox at a concentration of 7 mg/mL over 30 s (7.5 mg/kg). Three images were acquired before the Dox administration to establish background fluorescence. (*B*) Temporal evaluation of Dox extravasation with and without FUS-BTB disruption. C_v and C_e are the mean pixel intensity of the vessel and the extravascular space, respectively. The center of the region of interest (20 × 20 pixels) was 20 µm from the vessel wall. The plots show means ± SEM ($n = 4$ for each condition, i.e., non-FUS and FUS). The maximum mean fluorescence for the FUS and non-FUS was 0.52 ± 0.15 and 0.07 ± 0.02, a sevenfold difference. (*C*) Dox penetration from a line profile perpendicular to vessel wall (red dotted arrow in *A*). The plot shows the normalized maximum intensity projection (MIP) across the series of images. The dotted line shows a regression fitted to the data from four different animals for each condition (non-FUS and FUS). (*D*) Representative data of the temporal evolution of the normalized intensity of the line profile (red dotted arrow in *A*). For consistency in the notation of the experiments/modeling, C_v is the Dox intensity/concentration in the vessel, C_e is the Dox intensity/concentration in the extracellular/interstitial space.

convection-dominated transport as opposed to decreasing drug concentration as a function of distance from the vessel in diffusion-dominated transport).

FUS in Combination with Microbubbles Increases Early Extravasation and Penetration of T-DM1. Next, we assessed the intratumoral delivery of the antibody–drug conjugate T-DM1 after FUS-mediated BBB/BTB disruption. T-DM1 represents an antibody-based targeted chemotherapy and has recently shown promising preclinical outcomes in *HER2*-amplified BT474 breast cancer BMs (10). T-DM1 has significantly larger molecular size compared with the nontargeted doxorubicin (66.5 kDa vs. 580 Da), and the cellular uptake is receptor mediated (24, 27, 38, 39). Of note, the activity of T-DM1 in the brain microenvironment has been shown to be largely mediated by the chemotherapy component, whereas trastuzumab serves as vehicle for targeted transport in HER2-positive BMs (10). Intratumoral delivery and penetration of T-DM1 was investigated after staining for human IgG, as previously described (10). Immunostaining at 4 h post–T-DM1 administration showed significant increase in drug extravasation and tumor delivery ($P = 0.035$), when FUS sonication was performed immediately before drug injection, compared with mice that did not receive FUS (Fig. 3). Quantification of T-DM1 distance from tumor vessels revealed significant ($P = 0.007$) increase in drug penetration (mean ± SEM, 42 ± 7 vs. 11 ± 6 μm) after FUS compared with control (non-FUS) (Fig. 3*B*). Despite the early increase in drug delivery and tumor penetration, at 5 d postsonication the differences between the two groups diminished, as the BBB/BTB returns to baseline level relatively fast compared with the drug circulation time (4–6 h vs. 5 d) (40–45).

Quantification of Transvascular Transport via Mathematical Modeling Demonstrates Up to Fourfold Increase in Effective Diffusion Coefficient and Hydraulic Conductivity After FUS-Mediated BBB/BTB Disruption. While the above experimental findings provide important and previously unreported information at the cellular level about the intratumoral PK of drugs when combined with FUS, the relative importance of different transport mechanisms within the brain microenvironment remains largely unclear. To determine the relevance of different transport mechanisms, we combined two classes of mathematical models. First, the experimental data on vascular and interstitial drug PK was used to parameterize 2D tumor cord PBPK models for the two chemotherapeutic agents (46, 47) (Fig. 4 and *SI Appendix*). Multiple parameterizations for different experimental conditions allowed characterization of interexperimental variability. The models explicitly account for the distinct transcellular transport and retention of the drugs studied (nontargeted and antibody-based targeted chemotherapy; Fig. 4*A*). In the 2D tumor cord models (Fig. 4 *A* and *B* and *SI Appendix*, *Methods*, section 6, and Fig. S3), the model parameters were fitted using data from the temporal evaluation of doxorubicin extravasation after FUS-mediated BBB/BTB disruption (Fig. 2*B*), and a set of model parameters from the literature (see *SI Appendix*, Table S3 for values and references), as an initial estimate for the optimization procedure (*SI Appendix*). As our experimental quantification did not discriminate between free doxorubicin and doxorubicin bound to albumin, we did not include binding in our model, which reduced the parameter space in the fitting procedure. We achieved a good agreement between model output and the time-dependent doxorubicin extravasation traces for all of the experiments modeled (Fig. 4*B*), which indicates that the mathematical formulation captures the main mechanisms governing doxorubicin pharmacokinetics in the brain tumor microenvironment. The fitted model parameters (Table 1) indicated that only the vessel effective diffusion coefficient (4.3-fold increase, $P = 0.002$) and the hydraulic conductivity (4.5-fold increase, $P = 0.006$) were significantly different between the FUS and the control group (non-FUS) (Fig. 4*C* and Table 1). The estimated Peclet number in the interstitial subdomain for these model parameters increased from $Pe_{non\text{-}FUS} = 1.01 \times 10^{-1} \pm 2.75 \times 10^{-2}$ to $Pe_{FUS} = 22.15 \pm 15.45$ (mean ± SEM) after FUS, providing quantitative confirmation of the experimental observation (Fig. 2*D*) concerning the shift in drug pharmacokinetics in the interstitial space from diffusion-dominated to convection-dominated transport after FUS.

To fit the parameters of the time-dependent model to the static immunostaining images for T-DM1 (Fig. 3*A*), we established a methodology that allowed us to approximate the T-DM1 pharmacokinetics in the interstitium using the immunostaining data using the experimentally determined penetration and an analytic solution of the 1D advection–diffusion problem (*SI Appendix*). Using this approach, a good fit between the model and the reference solution was achieved (Fig. 4*B*). The fitted model parameters (Table 2) indicated that only the hydraulic conductivity (2.7-fold increase; $P = 0.003$) was significantly different between FUS and control (Fig. 4*C* and Table 2).

FUS in Combination with Microbubbles Leads to High Transvascular Flux for a Relatively Narrow Vessel Wall Pore Size Range and Increases Drug Penetration in the Brain Tumor Microenvironment. To study the influence of tumor's vascular heterogeneity on interstitial drug transport after FUS, we employed a percolation model (24, 48, 49) (Fig. 5*A* and *SI Appendix*, *Methods*, section 7), parameterized with the experiment-specific and drug-specific (fitted) model parameters (Fig. 4*C*, Tables 1 and 2, and *SI Appendix*, Table S5). The model showed lower drug gradients for the FUS-treated group in addition to significantly higher drug delivery and penetration, compared with non-FUS group (Fig.

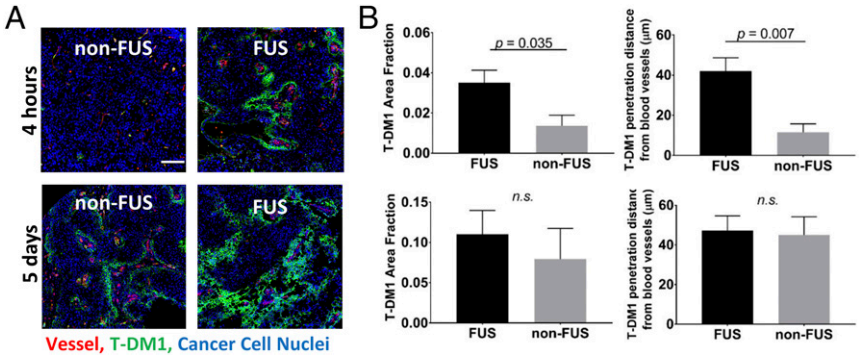

Fig. 3. FUS-BTB disruption increases early extravasation and penetration of T-DM1 in BT474-Gluc brain tumors. (*A*) Representative microscopy data of T-DM1 extravasation with and without FUS at 4 h and 5 d. (*B*) Quantification of the T-DM1 extravasation (*Left*) and penetration (*Right*) with and without FUS at 4 h (*Upper*) and 5 d (*Lower*) posttreatment. The plots show means ± SEM ($n = 6$). (Scale bar, 100 μm.) Parametric Student's *t* test for $P < 0.05$ (Prism 6; GraphPad). n.s., not significant.

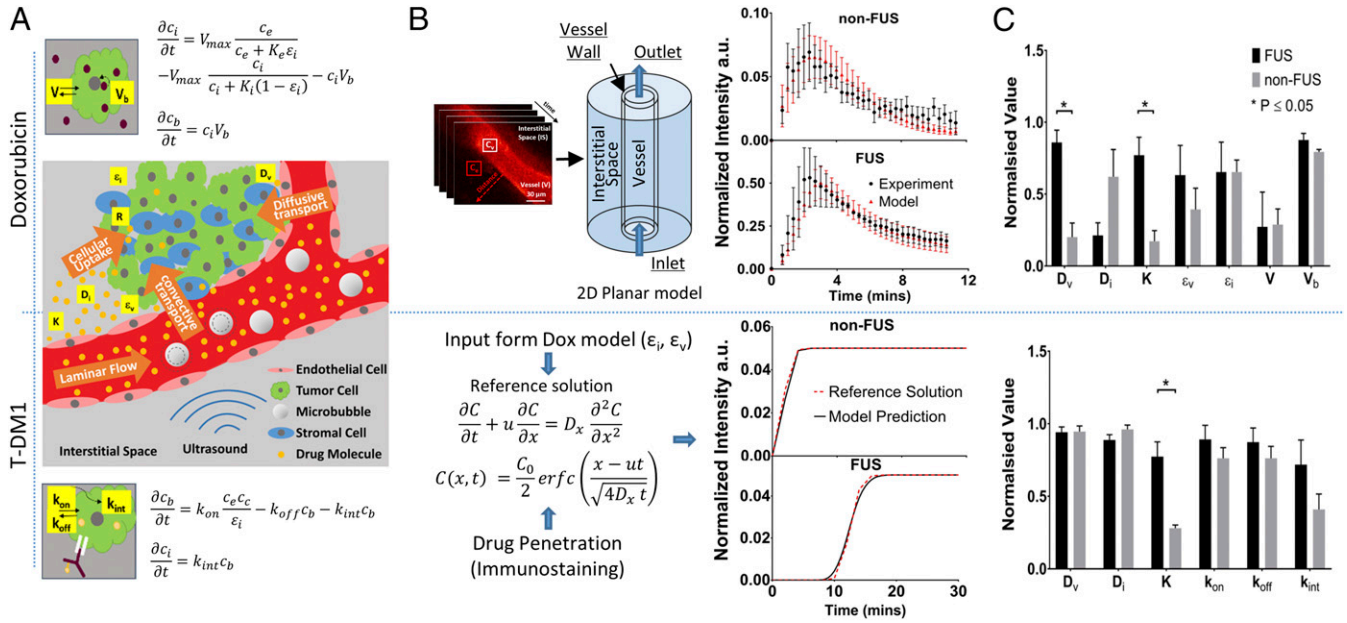

Fig. 4. Quantification of transvascular transport via mathematical modeling demonstrates multifold increase in effective diffusion coefficient (4.3-fold) and in hydraulic conductivity (4.5-fold) after FUS-BTB disruption. Vascular perfusion and cellular transport dictate interstitial drug transport after FUS-BTB disruption in BT474-Gluc brain tumors. (*A*) Schematic illustrating the transport of the anticancer agents from the vessel to the interstitial space along with the studied model parameters and agent-specific cellular uptake model equations. (*Upper*) Convection–diffusion–reaction model following Michaelis–Menten kinetics with binding of doxorubicin to DNA (V_b). (*Lower*) Convection–diffusion–reaction model for T-DM1. Excellent fit was observed for both doxorubicin and T-DM1. (*B*, *Upper*) The time dependence of doxorubicin extravasation from the fitted and experimental data for non-FUS and FUS-BBB/BTB disruption groups. (*B*, *Lower*) Parameter fit methodology for T-DM1 and fitted data from two different experiments. The fitted vascular and interstitial effective porosity (fraction of surface area occupied by pores) from the doxorubicin model was used as input to the T-DM1 fitting (i.e., same animal model). (*C*) Normalized parameter fit for non-FUS and FUS-BBB/BTB disruption groups (*Upper*, doxorubicin; *Lower*, T-DM1). The values for each parameter were normalized to maximum to be displayed on the same plot. The exact numbers and their units are shown in Tables 1 and 2 for doxorubicin and T-DM1, respectively. The plots show means ± SEM from fitted values from four different experiments for each condition.

5*A* and Table 3). The degree of perfusion in different parts of the network had significant impact on interstitial drug PK of the two drugs. Most notably, at poorly perfused vessels, T-DM1 had very low extravasation due to limited convective transport, whereas doxorubicin had very high extravasation due to diffusion-dominated transport (Fig. 5*A*). Interestingly, poorly perfused vessels (displaying a negative transvascular pressure) that are adjacent to highly perfused vessels (displaying a positive transvascular pressure) act as a drug sink for both drugs (Fig. 5*A*), providing an additional mechanism to transport drugs in poorly perfused tumor regions.

Modeling revealed a narrow range of vessel pore sizes that maximize the transvascular flux for doxorubicin (pore diameter, 50 nm) (Fig. 5*B*). Moreover, assuming no intracellular uptake (neglecting the reaction term in PK modeling), the transvascular flux of doxorubicin changes by more than twofold, suggesting that the PK of molecules with similar molecular weight but different cellular uptake may strongly change after FUS-BBB/BTB disruption. In addition, these findings are in agreement with experimental evidence that suggests that the cancer vascular phenotype (i.e., vessel pore size) plays a key role in the extravasation of drugs with small molecular weight (50). Similar trends but with lower amplitude were observed in the non-FUS group (*SI Appendix*, Fig. S4). For T-DM1, transvascular flux increases as pore diameter increases up to 200 nm and saturates above 200 nm (Fig. 5*B*).

To gain further insight into the interstitial transport of the two different drugs tested in this study, we conducted a sensitivity analysis for a number of transport parameters (Fig. 5*C*). For doxorubicin, FUS with microbubbles completely eliminates the importance of BBB/BTB effective diffusion coefficient in extravascular cell drug uptake (comparing D_v sensitivity in Fig. 5*C*, *Left* and *Right*). As a result, the rate of cell transmembrane transport dominates the extravascular cell uptake, irrespective of the degree of perfusion. T-DM1 transport was found to be insensitive to the vessel effective diffusion coefficient, which is consistent with the fitted data (Fig. 4*C*). In high perfusion regions, T-DM1 delivery in the tumor interstitial space is dominated by the cell kinetics (i.e., association/dissociation) irrespective of FUS-BBB/BTB disruption. The relative importance of hydraulic

Table 1. Doxorubicin fitted parameters

Name	Description	Non-FUS	FUS	Unit	*P* value
D_v	Vessel effective diffusion coefficient	0.31 ± 0.15	1.33 ± 0.13	$\mu m^2/s$	0.002
D_i	Interstitium effective diffusion coefficient	79.47 ± 24.26	27.09 ± 11.32	$\mu m^2/s$	0.1
K	Interstitium hydraulic conductivity	$1.03 \times 10^{-14} \pm 4.43 \times 10^{-15}$	$4.61 \times 10^{-14} \pm 7.46 \times 10^{-15}$	$m^3 \cdot s/kg$	0.006
ε_v	Vessel wall effective porosity	0.28 ± 0.11	0.45 ± 0.15	—	0.383
ε_i	Interstitium effective porosity	0.63 ± 0.08	0.63 ± 0.20	—	0.999
V	Rate of transmembrane transport	308.66 ± 116.17	290.45 ± 260.27	nM/s	0.951
V_b	Rate of drug binds to cellular DNA	$1.59 \times 10^{-3} \pm 2.68 \times 10^{-5}$	$1.78 \times 10^{-3} \pm 9.09 \times 10^{-5}$	1/s	0.132

Table 2. T-DM1 fitted parameters

Name	Description	Non-FUS	FUS	Unit	*P* value
D_v	Vessel effective diffusion coefficient	$4.60 \times 10^{-3} \pm 1.87 \times 10^{-4}$	$4.58 \times 10^{-3} \pm 1.75 \times 10^{-4}$	$\mu m^2/s$	0.941
D_i	Interstitium effective diffusion coefficient	$4.90 \times 10^{-2} \pm 1.54 \times 10^{-3}$	$4.53 \times 10^{-2} \pm 1.86 \times 10^{-3}$	$\mu m^2/s$	0.174
K	Interstitium hydraulic conductivity	$1.02 \times 10^{-14} \pm 8.02 \times 10^{-16}$	$2.82 \times 10^{-14} \pm 3.71 \times 10^{-15}$	$m^3 \cdot s/kg$	0.003
k_{on}	Association rate	$9.49 \times 10^{2} \pm 9.10 \times 10^{1}$	$1.11 \times 10^{3} \pm 1.21 \times 10^{2}$	1/(M*s)	0.326
k_{off}	Dissociation rate	$1.48 \times 10^{-1} \pm 1.60 \times 10^{-2}$	$1.69 \times 10^{-1} \pm 1.90 \times 10^{-2}$	1/s	0.418
k_{int}	Internalization constant	$8.80 \times 10^{-4} \pm 2.29 \times 10^{-4}$	$1.54 \times 10^{-3} \pm 3.65 \times 10^{-4}$	1/s	0.174

conductivity seems to be significantly higher ($P_{\text{non-FUS}} = 0.04$, $P_{\text{FUS}} = 0.004$) in low perfusion tumor areas, albeit to a lesser extent after FUS. However, the relative importance of cellular kinetics is very high after FUS compared with control.

FUS in Combination with Microbubbles Increases Cellular Transmembrane Transport and Uptake of Doxorubicin. Intravital multiphoton microscopy allowed determination of doxorubicin cellular uptake after FUS (Fig. 6). Depending on their location, the cells were separated in two categories: endothelial cells (ECs) for cells that were lining the vessel wall (Fig. 6*A*) and extravascular tumor cells (EVCs) for cells that were at least 10 μm beyond the endothelial wall (Fig. 6*A*). To quantify these changes, we redefined the objective function in the parameter fit procedure using the measured endothelial cell kinetics and fitted for changes in the rate of cellular transmembrane transport by assuming well-mixed cell populations (*SI Appendix*) (51). Our results show a significant increase in the rate of cellular transmembrane transport (>800-fold) and drug binding to the nucleus

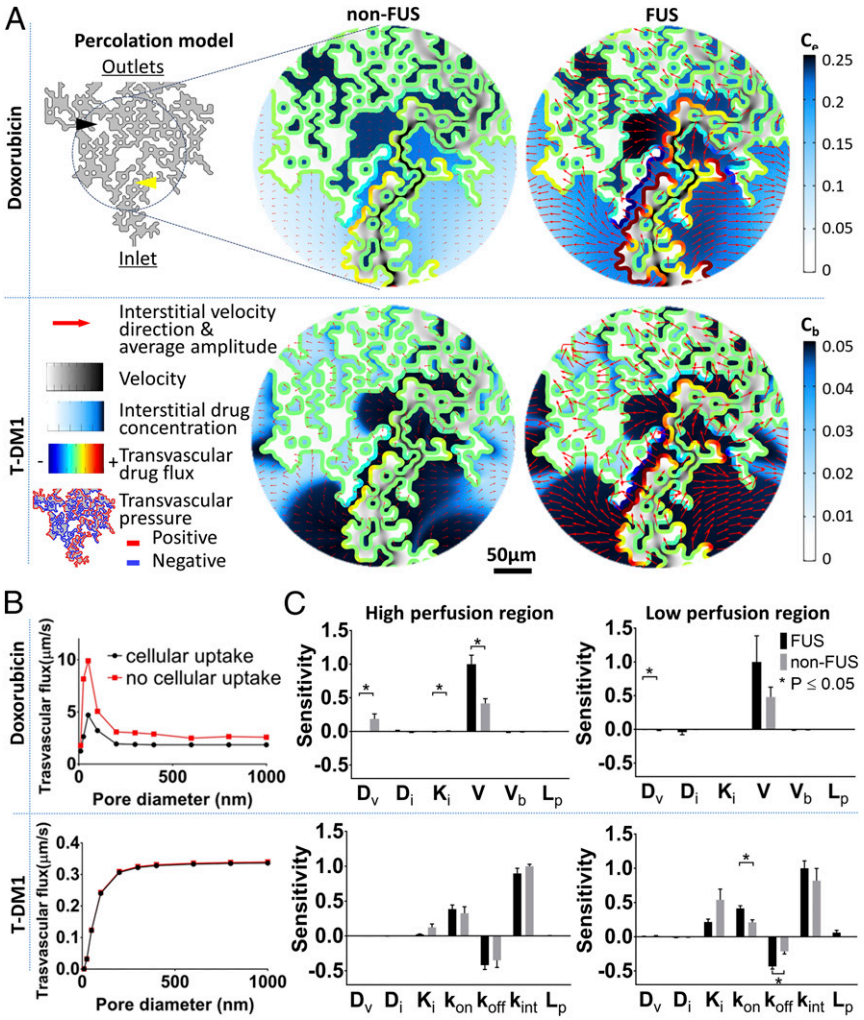

Fig. 5. Structurally heterogeneous mathematical tumor model predicts that FUS-BTB disruption overcomes transvascular transport barriers in brain tumor microenvironment and reveals the critical role of cancer cell transmembrane transport for effective uptake. (*A*) Modeling of vascular heterogenous perfusion using percolation model. Interstitial velocity, transvascular pressure difference (thresholded to highlight positive and negative regions), drug transvascular flux, and interstitial drug concentration captured at the time where drug reached its peak intensity [5 min for doxorubicin (Dox)—bolus administration—and 20 min for T-DM1]. The pore diameter used was 50 nm. (*B*) Transvascular flux for the Dox and T-DM1 (with FUS) with and without the cellular uptake. (*C*) Sensitivity analysis of the model parameters. The plots show means ± SEM from fitted values from four different experiments for each condition. The yellow arrow shows high perfusion region; the black arrow shows low perfusion region.

Table 3. Normalized SD of interstitial drug concentration

Dox	Non-FUS	FUS	T-DM1	Non-FUS	FUS
σ_{C_e}	0.35	0.2	σ_{C_e}	0.12	0.08
σ_{C_i}	0.07	0.04	σ_{C_i}	0.17	0.15
σ_{C_b}	0.07	0.04	σ_{C_b}	0.12	0.08

(>10-fold), compared with the baseline fitted value of the model shown in Table 1 (Fig. 6*C*). These data suggest that FUS in combination with microbubbles can increase the rate of transmembrane transport of doxorubicin in breast cancer cells, either directly via bubble–cell interactions (EC) or indirectly due to high drug concentration in the interstitial space.

Discussion

Here, we examined the impact of FUS-mediated BBB/BTB disruption on the transport of two anticancer agents in an orthotopic xenograft model of HER2-positive breast cancer BM using (*i*) intravital microscopy, (*ii*) immunostaining, and (*iii*) mathematical modeling of drug transport. As summarized in Table 4, this combined experimental and modeling study provides several insights regarding effective permeabilities of specific drugs through BBB/BTB, interstitial transport, and cell uptake/kinetics that were unknown to date despite the ongoing clinical evaluation of the FUS technology (21) (*SI Appendix*, Table S1).

In this study, we focused on the effects of FUS with microbubbles on delivery, penetration, and uptake of doxorubicin and T-DM1. We chose these drugs because (*i*) both are clinically relevant for the treatment of HER2-positive breast cancer (52–54), and (*ii*) they represent different classes of chemotherapeutic agents. Doxorubicin is a nontargeted, low–molecular-weight chemotherapeutic, while T-DM1 represents an antibody-based, targeted chemotherapeutic and is larger in size. Chemotherapeutic compounds were preferred over HER2 pathway signaling inhibitors, such as lapatinib or trastuzumab, since we have previously shown limited activity of HER2 pathway inhibitors in the brain microenvironment (9, 37). In the case of T-DM1, DM1 component mediates active cytotoxicity, whereas the antibody component serves as vehicle for the specific delivery of DM1 to tumor cells in the brain tumor microenvironment (10). Doxorubicin provides the advantage of autofluorescence over other nontargeting small-molecule chemotherapy agents, which allows intravital detection and measurement of drug pharmacokinetics without modification of the molecule. Our PBPK modeling accounted explicitly for the distinct transcellular transport and retention mechanisms of these drugs (Fig. 4*A*).

Intravital microscopy revealed that FUS has a profound impact on the penetration of the anticancer drug doxorubicin, as well as on cellular uptake rate in the brain microenvironment. Consistent with the physical mechanism of FUS-BBB/BTB disruption, we demonstrated significant effects of FUS on the effective diffusion coefficient and hydraulic conductivity with comprehensive and experimentally validated mathematical modeling. Due to the coupling between vascular and interstitial fluid of the model, the hydraulic conductivity parameter modulates transvascular flow (55). Therefore, the higher hydraulic conductivity post-FUS allows fluid to rapidly flow into the interstitial space. This is also in agreement with our experimental observations. Hence, FUS induces not only significant transient disruption of the BBB/BTB but also enhances the transport in the brain microenvironment.

To study the impact of structural heterogeneity in tumors on drug transport after FUS, we employed a percolation model (24). This model predicted a highly nonlinear and agent-specific relationship between vessel wall pore size and transvascular transport. Our results indicate that, for doxorubicin, the highest transvascular flux is achieved around vessel wall pore diameter of 50 nm. This is an important and unexpected finding, highlighting the impact that the differences between agent and vessel wall pore size have on transport (*SI Appendix*, Fig. S4). This finding can be leveraged to gain fundamental understanding of drug transport in the brain microenvironment, which may facilitate the development of more efficacious therapeutic protocols. Second, within that pore size range, the interaction of small molecules with cells (captured in the reaction term of our model) reduces the transvascular agent mass flux by approximately twofold compared with a nonreactive molecule. This finding suggests that the extravasation dynamics of surrogate molecules in the tumor microenvironment (i.e., nonreactive molecules) can differ significantly from the anticancer agents under study and may be very sensitive to the tumor vascular phenotype (i.e., vessel pore size). While experimental evidence shows that the K_{trans} and/or MRI contrast agent extravasation provides a reasonable surrogate of drug delivery ($R^2 < 0.77$; *SI Appendix*, Table S1), our data suggest that to improve the correlation between K_{trans} (or MRI contrast agent extravasation) and drug extravasation in brain tumors, the interaction of the molecules with the tumor microenvironment, in addition to their size, should be taken into consideration. Regarding recent research that demonstrated that the acoustic emissions can be used to control drug extravasation in brain tumors, our findings indicate that more work with drugs with different physical and chemical properties is needed to fully demonstrate the robustness of the method.

The sensitivity analysis indicated that an increase in the rate of BBB/BTB closure by 50% only results in a <1% increase in intracellular drug uptake by interstitial cells (see *SI Appendix*, *Methods*, section 7, for description and formulation). This suggests that multiple sonications at short time points after drug

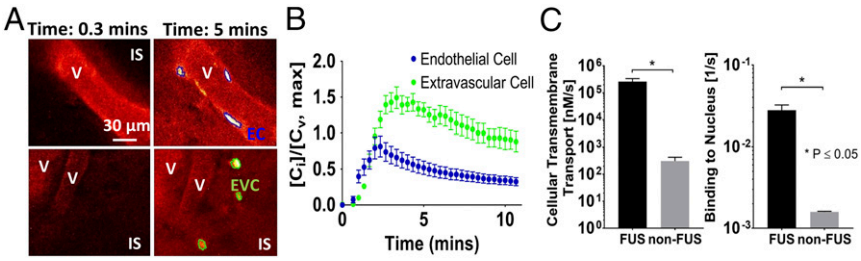

Fig. 6. FUS-BTB disruption increases doxorubicin transmembrane transport in endothelial and extravascular cells. (*A*) Representative doxorubicin images at 0.3 and 5 min after doxorubicin administration showing vessels, interstitial space (IS), and segmented endothelial (EC) and extravascular cells (EVC). (*B*) Quantification of intracellular doxorubicin kinetics for endothelial and interstitial cells. C_v is the doxorubicin intensity/concentration in the vessel, and C_i is the intracellular doxorubicin intensity/concentration. The plots show means ± SEM ($n = 6$) from each cell population. (*C*) Fitted rate of endothelial cellular transmembrane transport and drug bound to DNA.

Table 4. Insights revealed by the current combined experimental and modeling study

Tumor microenvironment	Effect of FUS with microbubbles
BBB/BTB permeability	Increase in effective permeability
Interstitial transport	Increase in convective transport
	Increase in penetration
	Decrease in drug gradients
Cellular uptake/kinetics	Increased rate of endothelial cell membrane transport
	Increased extravascular cell drug uptake
Drug	
Nontargeted chemotherapy (doxorubicin)	Increased extravasation and penetration
	Slow infusion (30 min) can lead up to a 40% higher peak cellular uptake.
	Therapies aimed to enhance cellular transmembrane kinetics can further improve drug uptake.
	Extravascular cell uptake reduces transvascular agent mass flux.
	This finding provides a possible explanation for the relatively poor correlation between MRI contrast agent imaging and drug extravasation that has been reported in the literature and tips toward the cautious use of imaging surrogates of drug delivery.
Targeted antibody-based chemotherapy (ADC T-DM1)	Increased early extravasation and penetration; however, effect was diminished 5 d after FUS.
	These findings may provide an additional explanation of why recent studies on FUS in combination with trastuzumab, etc., showed limited or statistically nonsignificant difference in the median animal survival after FUS-mediated BBB/BTB disruption, compared with non-FUS.

administration in brain tumors may not have the significant impact on cancer cell drug uptake, which was previously suggested using model parameters derived from healthy tissues (56).

The transient nature of FUS effects on vessels is particularly important for effective delivery of drugs, as inducing chronic BBB/BTB disruption can further increase IFP, which would inhibit the observed improved transport due decreased flow resistance. FUS has recently been shown to reduce IFP in extracranial tumors (20), suggesting that FUS can affect interstitial transport in a more direct way (57). Our study corroborates these findings and provides evidence that FUS contributes to enhanced interstitial convective transport in solid tumors, in addition to alleviating vascular barriers. In addition to these mechanisms, recent work suggested that FUS can expand the extracellular and perivascular spaces (58). Whereas this is a very important work in the field, studies were performed in healthy ex vivo rat brain slices. Likewise, targeted drug delivery studies with large molecules (e.g., AVV) and intravital microscopy with fluorescent nanoparticles demonstrating increased penetration after FUS-BBB disruption (45, 59), presumably due to enhanced interstitial convective transport, were performed in healthy mice.

Our model suggest that, for a given doxorubicin dose, if we use drug infusion for 45 min instead of a bolus administration, we can achieve a 40% increase in the cell uptake in the FUS-treated group (*SI Appendix*, *Methods*, section 8, and Fig. S5). This is because slow infusion allows to maintain a steady efficacious concentration for longer time, which leads to high drug internalization. Considering that the BBB/BTB remains open for at least 4 h after FUS-BBB/BTB disruption, we believe that this is a realistic scenario for the FUS-treated group (18). Given the narrow therapeutic window for current chemotherapeutics, this increase in tumor uptake could significantly improve efficacy.

While our model did not account for doxorubicin binding to albumin, the fast on/off binding kinetics of free and bound doxorubicin, relative to other processes in the model, such as cellular uptake (31), suggest that the limiting conditions identified by our model (i.e., cellular transmembrane transport) represent trends of the system. The reduction in the interstitial effective diffusion coefficient post-FUS, albeit not statistically significant, suggests that doxorubicin pharmacokinetics in the interstitial space are likely dominated by doxorubicin bound to albumin, which accounts for more than 75% of the chemotherapeutic in the circulation (31). The latter is consistent with the lower interstitial effective diffusion coefficient ($D_{control} = D_{FUS}/(1 + ([C]_{bound}/[C]_{free}))$) (31) and the higher contribution of convective transport for the larger molecular-weight albumin (580 Da vs. 66.5 kDa) in the FUS group. Incorporation of tumor molecular, spatial, and temporal phenotypic characteristics, including tumor type and cell line-specific expression of efflux pumps, diffusive permeability, and vascularity may provide additional insights with respect to drug transport mechanisms in the tumor core (5).

Regarding the impact of pressure, and by extension of microbubble effects, compared with previous studies in mice (citations in *SI Appendix*, refs. 25, 31, 37, 45–46, and 52) the pressure in our study was 30% lower when similar excitation frequencies were used (~1 MHz) and 30% higher when lower excitation frequencies were used (~0.5 MHz). Interestingly, in the present study, the mechanical index (M.I.), which is a metric that describes the strength of the mechanical effects of acoustic cavitation, was significantly lower than the M.I. reported in the above studies (0.47 vs. 0.58 ± 0.1), including studies in different disease models and animals (60). The use of low M.I. suggests that our findings provide conservative estimates of the impact of peak pressure on transvascular and interstitial transport parameters in the brain tumor microenvironment. While we anticipate stronger/weaker effects at higher/lower pressures, our current data do not allow us to draw firm conclusions. Future studies to explore the role of ultrasound exposure settings on drug transport are warranted.

Regarding larger targeted molecules, such as antibody-based therapies, our experimental data with T-DM1 show that, while there was a significant increase in early drug delivery and penetration at 4 h, this effect diminished at 5 d after FUS compared with control, supporting the hypothesis of T-DM1 accumulation is a result of the enhanced permeation (61). These findings may provide an additional explanation of why recent studies on FUS in combination with trastuzumab (43), or trastuzumab and pertuzumab (62), show limited or no significant difference in the median animal survival after FUS-mediated BBB/BTB disruption, compared with non-FUS. The sensitivity analysis indicated that improvement in extravascular cell uptake after FUS-BTB disruption can be attained by modifying the transmembrane transport, or by improving perfusion, by, for example, employing vascular normalization strategies (24). Interestingly, our model indicates that increasing drug dose benefits disproportionally the cellular uptake and penetration after FUS compared with control (non-FUS) (*SI Appendix*, Fig. S6). Our analysis (Fig. 5*B*) also

indicates that the transvascular flux increases almost linearly for BBB/BTB pore size diameter up to 50 nm and plateaus for higher pore sizes. While it remains unknown whether 50-nm pore sizes can be attained with FUS-BBB/BTB disruption, it is expected that pore sizes up to that level will lead to improved extravasation of small nanoparticles. More experimental and theoretical work in this direction is warranted.

Single-cell kinetics from intravital microscopy combined with mathematical modeling revealed a significant increase in the rate of transmembrane cellular transport of doxorubicin after FUS. This was the case for both vascular and extravascular cells. The doxorubicin concentration at the intracellular or extracellular space might influence the transvascular flux, in addition to the microbubble effects. Albeit not explicitly, our data capture this notion in two different ways. First, in FUS-treated animals, the extravascular cells (i.e., cells away from perfused vessels) demonstrate an abnormally high uptake of the doxorubicin (Fig. 6*A*), suggesting that the increased uptake is influenced by the drug concentration in extravascular space. Second, the mathematical modeling does not account explicitly for changes in the cell porosity; hence, the reported changes in transmembrane transport (Fig. 6*C*) should also encompass potential synergistic effects related to the doxorubicin dose, such as possible changes in the function of the dynamic influx/efflux transporter system at the BBB/BTB (12, 50, 63, 64).

There are several therapeutic implications of this observation. Whereas increased drug uptake by cancer cells may enhance the efficacy of therapeutic agents, FUS-mediated increase of drug uptake by vessel endothelial cells may be used to increase the delivery and activity of therapies that target abnormal modes of vascularization in brain tumors (12). For example, FUS could be utilized to increase the delivery of antiangiogenic agents, which would lengthen the time duration of vascular normalization and allow for enhanced penetration and efficacy of coadministered anticancer agents (8). Vascular co-option, a resistance mechanism to antiangiogenic therapy in glioblastoma, could also be more effectively targeted with agents delivered in conjunction with FUS that directly target cancer cells in contact with the normal blood vessels at the invasive front (8). In addition, FUS can also be employed to target therapy-resistant endothelial-like cells that support expansion of glioblastoma cells (65).

Apart from the transvascular, interstitial, and transcellular transport, there are additional physical properties of solid tumors that need to be investigated in combination with FUS and could be incorporated into our model. For example, "solid stress"—the abnormal mechanical force exerted by solid components of tumors (including brain tumors), that is, cells and matrix—may contribute to the complex transport processes in the brain/brain tumor microenvironment (66, 67). In addition to solid stress (exerted by solid tissue components), the inclusion of explicit modulation of IFP (exerted by fluid tissue components) (68) and potential lymphatic drainage (in the case of leptomeningeal tumors) (69) may allow for further elaboration of the significance of the potential transition from diffusion to convective transport after FUS. Reducing the uncertainty of the inferred parameters via reducing the number of parameters simultaneously fitted, increasing the number of experiments and tumor models, or experimentally validating the predicted values (70) can further consolidate our findings. Moreover, incorporation of mechanisms of cytotoxicity of the different agents may further improve the potential of the model to probe therapeutic efficacy. In addition, combining 3D imaging with imaging at depths higher than 150 μm will ensure that quantification of drug penetration and cellular uptake are free from the influence of out-of-plane vessels, providing more insights with respect to drug transport mechanisms in the tumor core. The latter might also allow improving the accuracy of the fitting procedures and of the extracted parameters and make even more robust the subsequent analysis of the drug PK using the percolation model. Finally, multiscale experimental methods can significantly contribute to furthering our understanding of drug PK in tumor microenvironment and allow us to further refine therapeutic interventions like FUS-BBB/BTB disruption (71). While improving drug delivery in BM is important, the brain microenvironment can confer de novo resistance to therapies (9) and should be taken into consideration for effective therapies.

Collectively, our study suggests that FUS in combination with microbubbles overcomes vascular and cellular transport barriers in the brain tumor microenvironment. Additionally, the combination of experimental data with PBPK modeling supports the hypothesis that FUS enhances interstitial transport in the brain tumor microenvironment by altering the drug delivery toward convective transport, resulting in increased tumor tissue penetration. Our approach provides a quantitative framework for the development of therapeutic protocols that aim to optimize FUS–drug combinations for maximization of drug penetration and uptake in BMs.

Methods

All animal procedures were performed according to the guidelines of the Public Health Policy on the Humane Care of Laboratory Animals and approved by the Institutional Animal Care and Use Committee of Massachusetts General Hospital. See *SI Appendix* for detailed information including in vivo experiment protocols, cell culture, FUS system transmission and characterization, image analysis, intravital microscopy, histology, mathematical models for drug transport, model parameter fit, sensitivity analysis, and numerical implementation.

ACKNOWLEDGMENTS. We thank T. J. Diefenbach and the Ragon Institute Imaging Core (Harvard Center for AIDS Research Immunology Core) for technical and instrumental support during microscopy studies, and Y. Zhang, M. Duquette, S. Roberge, P. Huang, and C. J. Smith for outstanding technical assistance in animal and histological studies. We also thank Drs. James Baish, Fan Yuan, and Triantafyllos Stylianopoulos for helpful comments on our manuscript. This study was supported in part by NIH Grants R00EB016971 (National Institute of Biomedical Imaging and Bioengineering) (to C.D.A.) and F31HL126449 (National Institute of Allergy and Infectious Diseases) (to M.D.), the Solidar-Immun Foundation (J.K.), and the German Research Foundation (Deutsche Forschungsgemeinschaft) Grant AS 422-2/1 (to V.A.). R.K.J. and D.F. are supported by National Cancer Institute Grants P01-CA080124, R01-CA208205, and U01-CA224348. R.K.J. is also supported by National Cancer Institute Grants R35-CA197743, P50-CA165962, and R01-CA129371, the Ludwig Center at Harvard, and the National Foundation for Cancer Research. N.M. is supported by National Cancer Institute Grant P01-CA174645.

1. Kodack DP, Askoxylakis V, Ferraro GB, Fukumura D, Jain RK (2015) Emerging strategies for treating brain metastases from breast cancer. *Cancer Cell* 27:163–175.
2. Lin X, DeAngelis LM (2015) Treatment of brain metastases. *J Clin Oncol* 33:3475–3484.
3. Sperduto PW, et al. (2012) Summary report on the graded prognostic assessment: An accurate and facile diagnosis-specific tool to estimate survival for patients with brain metastases. *J Clin Oncol* 30:419–425.
4. Kabraji S, et al. (2018) Drug resistance in HER2-positive breast cancer brain metastases: Blame the barrier or the brain? *Clin Cancer Res* 24:1795–1804.
5. Lockman PR, et al. (2010) Heterogeneous blood-tumor barrier permeability determines drug efficacy in experimental brain metastases of breast cancer. *Clin Cancer Res* 16:5664–5678.
6. Taskar KS, et al. (2012) Lapatinib distribution in HER2 overexpressing experimental brain metastases of breast cancer. *Pharm Res* 29:770–781.
7. Lyle LT, et al. (2016) Alterations in pericyte subpopulations are associated with elevated blood-tumor barrier permeability in experimental brain metastasis of breast cancer. *Clin Cancer Res* 22:5287–5299.
8. Jain RK (2014) Antiangiogenesis strategies revisited: From starving tumors to alleviating hypoxia. *Cancer Cell* 26:605–622.
9. Kodack DP, et al. (2017) The brain microenvironment mediates resistance in luminal breast cancer to PI3K inhibition through HER3 activation. *Sci Transl Med* 9: eaal4682.
10. Askoxylakis V, et al. (2015) Preclinical efficacy of ado-trastuzumab emtansine in the brain microenvironment. *J Natl Cancer Inst* 108:djv313.
11. Osswald M, et al. (2016) Impact of blood-brain barrier integrity on tumor growth and therapy response in brain metastases. *Clin Cancer Res* 22: 6078–6087.

12. Askoxylakis V, Arvanitis CD, Wong CSF, Ferraro GB, Jain RK (2017) Emerging strategies for delivering antiangiogenic therapies to primary and metastatic brain tumors. *Adv Drug Deliv Rev* 119:159–174.
13. Hendricks BK, Cohen-Gadol AA, Miller JC (2015) Novel delivery methods bypassing the blood-brain and blood-tumor barriers. *Neurosurg Focus* 38:E10.
14. Kroll RA, Neuwelt EA (1998) Outwitting the blood-brain barrier for therapeutic purposes: Osmotic opening and other means. *Neurosurgery* 42:1083–1099, discussion 1099–1100.
15. Gao X, et al. (2014) Overcoming the blood-brain barrier for delivering drugs into the brain by using adenosine receptor nanoagonist. *ACS Nano* 8:3678–3689.
16. Shahani K, et al. (2010) Injectable sustained release microparticles of curcumin: A new concept for cancer chemoprevention. *Cancer Res* 70:4443–4452.
17. Xing WK, Shao C, Qi ZY, Yang C, Wang Z (2015) The role of Gliadel wafers in the treatment of newly diagnosed GBM: A meta-analysis. *Drug Des Devel Ther* 9: 3341–3348.
18. Aryal M, Arvanitis CD, Alexander PM, McDannold N (2014) Ultrasound-mediated blood-brain barrier disruption for targeted drug delivery in the central nervous system. *Adv Drug Deliv Rev* 72:94–109.
19. McDannold N, Arvanitis CD, Vykhodtseva N, Livingstone MS (2012) Temporary disruption of the blood-brain barrier by use of ultrasound and microbubbles: Safety and efficacy evaluation in rhesus macaques. *Cancer Res* 72:3652–3663.
20. Arvanitis CD, Livingstone MS, Vykhodtseva N, McDannold N (2012) Controlled ultrasound-induced blood-brain barrier disruption using passive acoustic emissions monitoring. *PLoS One* 7:e45783.
21. Carpentier A, et al. (2016) Clinical trial of blood-brain barrier disruption by pulsed ultrasound. *Sci Transl Med* 8:343re2.
22. Stylianopoulos T, Munn LL, Jain RK (2018) Reengineering the physical microenvironment of tumors to improve drug delivery and efficacy: From mathematical modeling to bench to bedside. *Trends Cancer* 4:292–319.
23. Watson KD, et al. (2012) Ultrasound increases nanoparticle delivery by reducing intratumoral pressure and increasing transport in epithelial and epithelial-mesenchymal transition tumors. *Cancer Res* 72:1485–1493.
24. Stylianopoulos T, Jain RK (2013) Combining two strategies to improve perfusion and drug delivery in solid tumors. *Proc Natl Acad Sci USA* 110:18632–18637.
25. Dewhirst MW, Secomb TW (2017) Transport of drugs from blood vessels to tumour tissue. *Nat Rev Cancer* 17:738–750.
26. Baxter LT, Jain RK (1991) Transport of fluid and macromolecules in tumors. III. Role of binding and metabolism. *Microvasc Res* 41:5–23.
27. Schmidt MM, Wittrup KD (2009) A modeling analysis of the effects of molecular size and binding affinity on tumor targeting. *Mol Cancer Ther* 8:2861–2871.
28. Mitchell MJ, Jain RK, Langer R (2017) Engineering and physical sciences in oncology: Challenges and opportunities. *Nat Rev Cancer* 17:659–675.
29. Baxter LT, Jain RK (1989) Transport of fluid and macromolecules in tumors. I. Role of interstitial pressure and convection. *Microvasc Res* 37:77–104.
30. El-Kareh AW, Secomb TW (2000) A mathematical model for comparison of bolus injection, continuous infusion, and liposomal delivery of doxorubicin to tumor cells. *Neoplasia* 2:325–338.
31. Eikenberry S (2009) A tumor cord model for doxorubicin delivery and dose optimization in solid tumors. *Theor Biol Med Model* 6:16.
32. Chauhan VP, Jain RK (2013) Strategies for advancing cancer nanomedicine. *Nat Mater* 12:958–962.
33. Jain RK, Tong RT, Munn LL (2007) Effect of vascular normalization by antiangiogenic therapy on interstitial hypertension, peritumor edema, and lymphatic metastasis: Insights from a mathematical model. *Cancer Res* 67:2729–2735.
34. Thurber GM, et al. (2013) Single-cell and subcellular pharmacokinetic imaging allows insight into drug action in vivo. *Nat Commun* 4:1504.
35. Jain RK, Munn LL, Fukumura D (2002) Dissecting tumour pathophysiology using intravital microscopy. *Nat Rev Cancer* 2:266–276.
36. Lawson BAJ, et al. (2018) Unlocking data sets by calibrating populations of models to data density: A study in atrial electrophysiology. *Sci Adv* 4:e1701676.
37. Kodack DP, et al. (2012) Combined targeting of HER2 and VEGFR2 for effective treatment of HER2-amplified breast cancer brain metastases. *Proc Natl Acad Sci USA* 109:E3119–E3127.
38. Burris HA, 3rd, Tibbitts J, Holden SN, Sliwkowski MX, Lewis Phillips GD (2011) Trastuzumab emtansine (T-DM1): A novel agent for targeting HER2+ breast cancer. *Clin Breast Cancer* 11:275–282.
39. Lewis Phillips GD, et al. (2008) Targeting HER2-positive breast cancer with trastuzumab-DM1, an antibody-cytotoxic drug conjugate. *Cancer Res* 68:9280–9290.
40. Hynynen K, McDannold N, Vykhodtseva N, Jolesz FA (2001) Noninvasive MR imaging-guided focal opening of the blood-brain barrier in rabbits. *Radiology* 220:640–646.
41. Sheikov N, et al. (2006) Brain arterioles show more active vesicular transport of blood-borne tracer molecules than capillaries and venules after focused ultrasound-evoked opening of the blood-brain barrier. *Ultrasound Med Biol* 32:1399–1409.
42. Hynynen K, McDannold N, Sheikov NA, Jolesz FA, Vykhodtseva N (2005) Local and reversible blood-brain barrier disruption by noninvasive focused ultrasound at frequencies suitable for trans-skull sonications. *Neuroimage* 24:12–20.
43. Park E-J, Zhang Y-Z, Vykhodtseva N, McDannold N (2012) Ultrasound-mediated blood-brain/blood-tumor barrier disruption improves outcomes with trastuzumab in a breast cancer brain metastasis model. *J Control Release* 163:277–284.
44. Marty B, et al. (2012) Dynamic study of blood-brain barrier closure after its disruption using ultrasound: A quantitative analysis. *J Cereb Blood Flow Metab* 32:1948–1958.
45. Cho EE, Drazic J, Ganguly M, Stefanovic B, Hynynen K (2011) Two-photon fluorescence microscopy study of cerebrovascular dynamics in ultrasound-induced blood-brain barrier opening. *J Cereb Blood Flow Metab* 31:1852–1862.
46. Gerlowski LE, Jain RK (1983) Physiologically based pharmacokinetic modeling: Principles and applications. *J Pharm Sci* 72:1103–1127.
47. Baxter LT, Yuan F, Jain RK (1992) Pharmacokinetic analysis of the perivascular distribution of bifunctional antibodies and haptens: Comparison with experimental data. *Cancer Res* 52:5838–5844.
48. Baish JW, et al. (1996) Role of tumor vascular architecture in nutrient and drug delivery: An invasion percolation-based network model. *Microvasc Res* 51:327–346.
49. Chauhan VP, et al. (2012) Normalization of tumour blood vessels improves the delivery of nanomedicines in a size-dependent manner. *Nat Nanotechnol* 7:383–388.
50. Phoenix TN, et al. (2016) Medulloblastoma genotype dictates blood brain barrier phenotype. *Cancer Cell* 29:508–522.
51. Beerenwinkel N, Schwarz RF, Gerstung M, Markowetz F (2015) Cancer evolution: Mathematical models and computational inference. *Syst Biol* 64:e1–e25.
52. Rayson D, et al. (2008) Anthracycline-trastuzumab regimens for HER2/neu-overexpressing breast cancer: Current experience and future strategies. *Ann Oncol* 19:1530–1539.
53. Turner N, Biganzoli L, Di Leo A (2015) Continued value of adjuvant anthracyclines as treatment for early breast cancer. *Lancet Oncol* 16:e362–e369.
54. Verma S, et al.; EMILIA Study Group (2012) Trastuzumab emtansine for HER2-positive advanced breast cancer. *N Engl J Med* 367:1783–1791.
55. Netti PA, Roberge S, Boucher Y, Baxter LT, Jain RK (1996) Effect of transvascular fluid exchange on pressure-flow relationship in tumors: A proposed mechanism for tumor blood flow heterogeneity. *Microvasc Res* 52:27–46.
56. Nhan T, Burgess A, Lilge L, Hynynen K (2014) Modeling localized delivery of doxorubicin to the brain following focused ultrasound enhanced blood-brain barrier permeability. *Phys Med Biol* 59:5987–6004.
57. Frenkel V (2008) Ultrasound mediated delivery of drugs and genes to solid tumors. *Adv Drug Deliv Rev* 60:1193–1208.
58. Hersh DS, et al. (2016) Pulsed ultrasound expands the extracellular and perivascular spaces of the brain. *Brain Res* 1646:543–550.
59. Wang S, et al. (2017) Non-invasive, focused ultrasound-facilitated gene delivery for optogenetics. *Sci Rep* 7:39955.
60. Chu P-C, et al. (2016) Focused ultrasound-induced blood-brain barrier opening: Association with mechanical index and cavitation index analyzed by dynamic contrast-enhanced magnetic-resonance imaging. *Sci Rep* 6:33264.
61. Jain RK, Stylianopoulos T (2010) Delivering nanomedicine to solid tumors. *Nat Rev Clin Oncol* 7:653–664.
62. Kobus T, Zervantonakis IK, Zhang Y, McDannold NJ (2016) Growth inhibition in a brain metastasis model by antibody delivery using focused ultrasound-mediated blood-brain barrier disruption. *J Control Release* 238:281–288.
63. Abbott NJ, Rönnbäck L, Hansson E (2006) Astrocyte-endothelial interactions at the blood-brain barrier. *Nat Rev Neurosci* 7:41–53.
64. Banks WA (2016) From blood-brain barrier to blood-brain interface: New opportunities for CNS drug delivery. *Nat Rev Drug Discov* 15:275–292.
65. Borovski T, et al. (2013) Therapy-resistant tumor microvascular endothelial cells contribute to treatment failure in glioblastoma multiforme. *Oncogene* 32:1539–1548.
66. Nia HT, et al. (2016) Solid stress and elastic energy as measures of tumour mechanopathology. *Nat Biomed Eng* 1:0004.
67. Nia HT, et al. (2018) Quantifying solid stress and elastic energy from excised or in situ tumors. *Nat Protoc* 13:1091–1105.
68. Jain RK (1987) Transport of molecules in the tumor interstitium: A review. *Cancer Res* 47:3039–3051.
69. Louveau A, et al. (2015) Structural and functional features of central nervous system lymphatic vessels. *Nature* 523:337–341.
70. Mittapalli RK, et al. (2017) Quantitative fluorescence microscopy measures vascular pore size in primary and metastatic brain tumors. *Cancer Res* 77:238–246.
71. Cui M, et al. (2017) A proof-of-concept study for developing integrated two-photon microscopic and magnetic resonance imaging modality at ultrahigh field of 16.4 tesla. *Sci Rep* 7:2733.